

## An 8.0% Determination of the Baryon Fraction in the Intergalactic Medium from Localized Fast Radio Bursts

BAO WANG <sup>1,2,3</sup> AND JUN-JIE WEI <sup>1,2</sup>

<sup>1</sup>*Purple Mountain Observatory, Chinese Academy of Sciences, Nanjing 210023, China*

<sup>2</sup>*School of Astronomy and Space Sciences, University of Science and Technology of China, Hefei 230026, China*

<sup>3</sup>*School of Physics and Electronics, Hunan Normal University, Changsha 410081, China*

### ABSTRACT

The dispersion measure (DM)–redshift relation of fast radio bursts (FRBs) has been proposed as a potential new tool for probing intergalactic medium (IGM) and for studying cosmology. However, the poor knowledge of the baryon fraction in the IGM ( $f_{\text{IGM}}$ ) and its degeneracy with cosmological parameters impose restrictions on the cosmological applications of FRBs. Furthermore, DMs contributed by the IGM ( $\text{DM}_{\text{IGM}}$ ) and host galaxy ( $\text{DM}_{\text{host}}$ ), important cosmological quantities, cannot be exactly extracted from observations, which would bring uncontrolled systematic uncertainties in FRB cosmology. In this work, we use seventeen localized FRBs to constrain  $f_{\text{IGM}}$  and its possible redshift evolution. Other cosmological probes such as type Ia supernovae, baryon acoustic oscillations, and cosmic microwave background radiation are combined to break parameter degeneracy. Taking into account the probability distributions of  $\text{DM}_{\text{IGM}}$  and  $\text{DM}_{\text{host}}$  derived from the the IllustrisTNG simulation, we obtain a robust measurement of  $f_{\text{IGM}} = 0.927 \pm 0.075$ , representing a precision of 8.0%. We find that there is no strong evidence for the redshift dependence of  $f_{\text{IGM}}$  at the current observational data level. The rapid progress in localizing FRBs will significantly improve the constraints on  $f_{\text{IGM}}$ .

*Keywords:* Radio transient sources (2008) — Intergalactic medium (813) — Observational cosmology (1146) — Cosmological parameters (339)

### 1. INTRODUCTION

Fast radio bursts (FRBs) are a class of brief ( $\sim$ ms) and intense ( $\sim$ Jy) radio transients with large dispersion measures (DMs), well in excess of the expected contributions from the Milky Way (Lorimer et al. 2007; Thornton et al. 2013; Petroff et al. 2016; Platts et al. 2019; Xiao et al. 2021; Zhang 2022). Owing to their anomalously high DMs, FRBs are believed to be of extragalactic or even cosmological origin. To date, more than 600 FRBs have been detected, and over two dozen of them have been reported to repeat (CHIME/FRB Collaboration et al. 2021). There are more than 20 FRBs with definite host galaxies and redshift measurements. These observations suggest that FRBs are promising tools for studying cosmology. Some proposals include using localized FRBs to measure the baryon number density of the universe (Deng & Zhang 2014; McQuinn 2014; Macquart et al. 2020; Yang et al. 2022), constrain the dark energy equation of state (Gao et al. 2014; Zhou et al. 2014; Walters et al. 2018; Wei et al.

2018; Zhao et al. 2020; Qiu et al. 2022), constrain cosmic reionization history (Deng & Zhang 2014; Zheng et al. 2014; Hashimoto et al. 2021), measure cosmological distance (Yu & Wang 2017; Kumar & Linder 2019), or measure the Hubble constant (Hagstotz et al. 2022; Wu et al. 2022); using strongly lensed FRBs to probe the nature of compact dark matter (Muñoz et al. 2016; Wang & Wang 2018), or measure the Hubble constant and cosmic curvature (Li et al. 2018).

Another cosmological puzzle is the baryon distribution of the universe. While it is widely believed that more than three-quarters of the baryonic content of the universe resides in the diffuse intergalactic medium (IGM), with only a small fraction in galaxies and galaxy clusters (Fukugita et al. 1998; Cen & Ostriker 2006), gaining direct observational evidence of the baryon distribution is challenging. There have been many studies of detecting the baryon fraction in the IGM,  $f_{\text{IGM}}$ , through numerical simulations (Cen & Ostriker 1999, 2006; Meiksin 2009) or observations (Fukugita et al. 1998; Fukugita & Peebles 2004; Shull et al. 2012; Hill et al. 2016; Muñoz & Loeb 2018). For instance, Meiksin (2009) performed numerical simulations and suggested that  $\sim 90\%$  of the baryons produced by the Big Bang are contained within the IGM at redshifts of  $z \geq 1.5$  (i.e.,  $f_{\text{IGM}} \approx 0.9$ ). It was

observed that  $18 \pm 4\%$  of the baryons exists in galaxies, circumgalactic medium, intercluster medium, and cold neutral gas at  $z \leq 0.4$ , or equivalently  $f_{\text{IGM}} \approx 0.82$  (Shull et al. 2012). There is an ongoing debate about the value of  $f_{\text{IGM}}$ .

The observed DMs of cosmological FRBs are mainly contributed by the IGM. Since the DM contributed by the IGM ( $\text{DM}_{\text{IGM}}$ ) carries important information on the location of baryons in the late universe, one may combine the  $\text{DM}_{\text{IGM}}$  and  $z$  information of FRBs to constrain the IGM baryon fraction  $f_{\text{IGM}}$ . Indeed, a number of methods have been proposed to estimate  $f_{\text{IGM}}$  by utilizing the  $\text{DM}(z)$  data of FRBs (Li et al. 2019, 2020; Wei et al. 2019; Walters et al. 2019; Qiang & Wei 2020; Dai & Xia 2021; Lin et al. 2022; Lemos et al. 2022). However, one issue that restricts such studies is the strong degeneracy between cosmological parameters and  $f_{\text{IGM}}$ . It is hard to determine  $f_{\text{IGM}}$  directly only relying on FRB data. Moreover, there is another thorny issue that DMs contributed by FRB host galaxies ( $\text{DM}_{\text{host}}$ ) and the inhomogeneities in the IGM ( $\text{DM}_{\text{IGM}}$ ) cannot be exactly extracted from observations (Macquart et al. 2020). Previous studies assumed fixed values for them, which would bring uncontrollable systematic uncertainties in the analysis. A more plausible approach is to treat them as probability distributions derived from cosmological simulations (Jaroszynski 2019; Macquart et al. 2020; Zhang et al. 2020, 2021; Wu et al. 2022).

In this paper, we present a high-precision measurement of the baryon fraction in the IGM with seventeen localized FRBs through the  $\text{DM}_{\text{IGM}}-z$  relation. In order to break the degeneracy between cosmological parameters and  $f_{\text{IGM}}$ , we combine FRB data with current constraints from type Ia supernovae (SNe Ia), baryon acoustic oscillations (BAOs), and cosmic microwave background (CMB) radiation. In our  $f_{\text{IGM}}$  estimation, the reasonable probability distributions of  $\text{DM}_{\text{host}}$  and  $\text{DM}_{\text{IGM}}$  derived from the IllustrisTNG simulation (Zhang et al. 2020, 2021) are adopted to reduce the systematic errors. Additionally, to explore the possible evolution of  $f_{\text{IGM}}$  with redshift, we also consider two different parametric models, namely a constant model and a time-dependent model.

The rest of our paper is organized as follows. In Section 2, we review the FRB DM measurements and the probability distributions of  $\text{DM}_{\text{host}}$  and  $\text{DM}_{\text{IGM}}$  derived from the IllustrisTNG simulation. In Section 3, we give an introduction of the compilations of the three other cosmological probes, including SNe Ia, BAO, and CMB. Monte Carlo Markov Chain (MCMC) parameter inference results are presented in Section 4. Finally, conclusions are summarized in Section 5.

## 2. FRB DISPERSION MEASURES

The precise localization of FRBs to their host galaxies provides an ensemble of DM and  $z$  measurements. The DM measurement represents the integrated column density of free electrons along the line of sight. For an extragalactic FRB,

its observed DM can be separated into the following components:

$$\text{DM}_{\text{obs}}(z) = \text{DM}_{\text{ISM}}^{\text{MW}} + \text{DM}_{\text{halo}}^{\text{MW}} + \text{DM}_{\text{IGM}}(z) + \frac{\text{DM}_{\text{host}}}{1+z}, \quad (1)$$

where  $\text{DM}_{\text{ISM}}^{\text{MW}}$ ,  $\text{DM}_{\text{halo}}^{\text{MW}}$ ,  $\text{DM}_{\text{IGM}}$ , and  $\text{DM}_{\text{host}}$  represent the DM contributions from the Milky Way interstellar medium (ISM), the Milky Way halo, the IGM, and the FRB host galaxy, respectively. The  $(1+z)$  factor converts the local  $\text{DM}_{\text{host}}$  to the observed one (Deng & Zhang 2014). Because of the inhomogeneity of the free electron distribution in the IGM, two sources at the same redshift but in different sightlines will likely have significant differences in the measured value of  $\text{DM}_{\text{IGM}}$ . Adopting the flat  $\Lambda$ CDM cosmological model, the average value of  $\text{DM}_{\text{IGM}}$  can be estimated as (Deng & Zhang 2014)

$$\langle \text{DM}_{\text{IGM}} \rangle(z) = \frac{3c\Omega_b H_0}{8\pi G m_p} \int_0^z \frac{(1+z') f_{\text{IGM}}(z') \chi_e(z')}{\sqrt{\Omega_m (1+z')^3 + 1 - \Omega_m}} dz', \quad (2)$$

where  $m_p$  is the proton mass,  $H_0$  is the Hubble constant,  $f_{\text{IGM}}(z)$  is the baryon fraction in the IGM, and  $\Omega_b$  and  $\Omega_m$  are the present-day baryon and matter density parameters. The free electron number fraction per baryon is  $\chi_e(z) = \frac{3}{4}\chi_{e,\text{H}}(z) + \frac{1}{8}\chi_{e,\text{He}}(z)$ , where  $\chi_{e,\text{H}}(z)$  and  $\chi_{e,\text{He}}(z)$  are the ionization fractions of hydrogen and helium, respectively. Both hydrogen and helium are completely ionized at redshifts  $z < 3$  (Meiksin 2009; Becker et al. 2011), allowing one to set  $\chi_{e,\text{H}} = \chi_{e,\text{He}} = 1$ , which gives  $\chi_e = 7/8$ .

The  $\text{DM}_{\text{IGM}}$  value of a well-localized FRB can be extracted using  $\text{DM}_{\text{IGM}} = \text{DM}_{\text{obs}} - \text{DM}_{\text{ISM}}^{\text{MW}} - \text{DM}_{\text{halo}}^{\text{MW}} - \text{DM}_{\text{host}}/(1+z)$ . Here the  $\text{DM}_{\text{ISM}}^{\text{MW}}$  term can be well estimated from the NE2001 model of the ISM free electron distribution (Cordes & Lazio 2002). The  $\text{DM}_{\text{halo}}^{\text{MW}}$  term is not well constrained, but is expected to contribute  $50 \sim 80 \text{ pc cm}^{-3}$  (Prochaska & Zheng 2019). Hereafter we assume that the probability distribution of  $\text{DM}_{\text{halo}}^{\text{MW}}$  can be described by a Gaussian distribution with mean  $\mu_{\text{halo}} = 65 \text{ pc cm}^{-3}$  and standard deviation  $\sigma_{\text{halo}} = 15 \text{ pc cm}^{-3}$  (Wu et al. 2022):

$$P_{\text{halo}}(\text{DM}_{\text{halo}}^{\text{MW}}) = \frac{1}{\sqrt{2\pi}\sigma_{\text{halo}}} \exp\left[-\frac{(\text{DM}_{\text{halo}}^{\text{MW}} - \mu_{\text{halo}})^2}{2\sigma_{\text{halo}}^2}\right]. \quad (3)$$

Based on the state-of-the-art IllustrisTNG simulation (Springel et al. 2018), Zhang et al. (2020) selected a large sample of simulated galaxies with similar properties to observed FRB hosts to derive the distributions of  $\text{DM}_{\text{host}}$  of repeating and non-repeating FRBs. The distributions of  $\text{DM}_{\text{host}}$  can be well described by the log-normal function (Macquart et al. 2020; Zhang et al. 2020)

$$P_{\text{host}}(\text{DM}_{\text{host}}) = \frac{1}{\sqrt{2\pi}\text{DM}_{\text{host}}\sigma_{\text{host}}} \exp\left[-\frac{(\ln \text{DM}_{\text{host}} - \mu_{\text{host}})^2}{2\sigma_{\text{host}}^2}\right], \quad (4)$$

where  $e^{\mu_{\text{host}}}$  and  $e^{2\mu_{\text{host}}+\sigma_{\text{host}}^2}(e^{\sigma_{\text{host}}^2}-1)$  are the mean and variance of the distribution, respectively. Due to the diversity of host galaxies, Zhang et al. (2020) computed the  $\text{DM}_{\text{host}}$  distributions for repeating FRBs in dwarf galaxies (like FRB 121102, FRB 180301, FRB 181030, and FRB 190711), repeating FRBs in spiral galaxies (like FRB 180916 and FRB 201124), and non-repeating FRBs separately. Here we divide the localized FRBs into these three types according to their host properties. The evolution of the median of  $\text{DM}_{\text{host}}$  ( $\mu_{\text{host}}$ ) can be fitted by  $e^{\mu_{\text{host}}}(z) = \kappa(1+z)^\gamma$ , where  $\kappa$  and  $\gamma$  are given by Zhang et al. (2020). The propagated uncertainty  $\sigma_{\text{host}}$  of  $\text{DM}_{\text{host}}$  is calculated from the uncertainties of  $\kappa$  and  $\gamma$ . With this expression of redshift evolution, we can derive the  $\text{DM}_{\text{host}}$  distributions at any redshift of a localized FRB.

To date, more than 20 FRBs have already been localized. Nonetheless, some of them are not available for our analysis. For example, the DM of FRB 181030 is only  $103.396 \text{ pc cm}^{-3}$  (Bhardwaj et al. 2021a), which will be reduced to a negative value after subtracting DM contributions from the Milky Way ISM and halo. That is, the integral upper limit ( $\text{DM}_{\text{E}} \equiv \text{DM}_{\text{obs}} - \text{DM}_{\text{ISM}}^{\text{MW}} - \text{DM}_{\text{halo}}^{\text{MW}}$ ) in the probability of the external DM contribution outside our Galaxy (see Equation (7)) will become negative. FRB 190520B is co-located with a compact, persistent radio source and associated with a dwarf host galaxy at a redshift of 0.241 (Niu et al. 2022). It is a clear outlier from the general trend of the extragalactic  $\text{DM}_{\text{E}}-z$  relation, with an unprecedented DM contribution from its host galaxy. Thus its  $\text{DM}_{\text{host}}$  term can not be accurately deducted. FRB 200110E is located in a globular cluster in the direction of the nearby galaxy M81 (Bhardwaj et al. 2021b; Kirsten et al. 2022). The distance of FRB 200110E is only 3.6 Mpc, and the IGM between the Milky Way and M81 contributes of the order of  $\text{DM}_{\text{IGM}} \approx 1 \text{ pc cm}^{-3}$ . Thus the cosmological information carried by FRB 200110E is too little. Additionally, the peculiar velocity effect is significant, which makes it can not be used for cosmological studies. After excluding these FRBs, we use a sample of 17 FRBs in the redshift range  $0.0337 \leq z \leq 0.66$  to constrain  $f_{\text{IGM}}(z)$ .<sup>1</sup> Table 1 lists the redshifts,  $\text{DM}_{\text{obs}}$ , and  $\text{DM}_{\text{ISM}}^{\text{MW}}$  of our sample. The estimated  $\text{DM}_{\text{IGM}}$  and measured  $z$  values for the 17 localized FRBs are shown in Figure 1. We have estimated  $\text{DM}_{\text{IGM}}$  by subtracting the following from the observed  $\text{DM}_{\text{obs}}$  value:  $\text{DM}_{\text{ISM}}^{\text{MW}}$  from the Galactic ISM model; a median of  $65 \text{ pc cm}^{-3}$  contributed by  $\text{DM}_{\text{halo}}^{\text{MW}}$ ; and a median value of  $\text{DM}_{\text{host}}$  at different redshifts estimated from the IllustrisTNG simulation (Zhang et al. 2020).

<sup>1</sup> After this work was done, we noticed a new article (Ryder et al. 2022), which has reported the discovery of a burst, FRB 220610A, in a complex host galaxy system at a redshift of  $z = 1.016$ . Whereas this burst was not included in our sample.

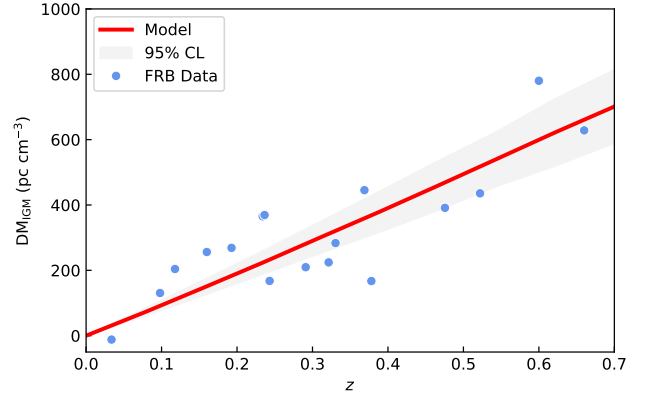


**Figure 1.** The  $\text{DM}_{\text{IGM}}-z$  relation for 17 localized FRBs. The data points are estimations of  $\text{DM}_{\text{IGM}}$  versus redshift measurements for the 17 localized FRBs. The  $\text{DM}_{\text{IGM}}$  values are estimated by correcting the observed  $\text{DM}_{\text{obs}}$  for the contributions from our galaxy and the FRB host galaxy (see the text for details). The solid line shows the model of Equation (2) with the inferred parameters of  $\Omega_m = 0.309 \pm 0.006$ ,  $\Omega_b h^2 = 0.02245 \pm 0.00013$ ,  $H_0 = 67.73 \pm 0.44 \text{ km s}^{-1} \text{ Mpc}^{-1}$ , and  $f_{\text{IGM},0} = 0.927 \pm 0.075$ . The shaded area represents the uncertainty of the estimated average  $\text{DM}_{\text{IGM}}$  value at the 95% confidence level due to the uncertainties of the inferred model parameters which we mentioned above.

**Table 1.** Properties of the 17 localized FRBs

Name	Redshift	$\text{DM}_{\text{obs}}$ ( $\text{pc cm}^{-3}$ )	$\text{DM}_{\text{ISM}}^{\text{MW}}$ ( $\text{pc cm}^{-3}$ )	Refs.
FRB 121102	0.19273	$557 \pm 2$	188.0	1
FRB 180301	0.3304	$536 \pm 0.2$	152.0	2
FRB 180916	0.0337	$349.349 \pm 0.005$	200.0	3
FRB 180924	0.3214	$361.42 \pm 0.06$	40.5	4
FRB 181112	0.4755	$589.27 \pm 0.03$	102.0	5
FRB 190102	0.291	$363.6 \pm 0.3$	57.3	6
FRB 190523	0.66	$760.8 \pm 0.6$	37.0	7
FRB 190608	0.1178	$338.7 \pm 0.5$	37.2	8
FRB 190611	0.378	$321.4 \pm 0.2$	57.83	9
FRB 190614	0.6	$959.2 \pm 0.5$	83.5	10
FRB 190711	0.522	$593.1 \pm 0.4$	56.4	9
FRB 190714	0.2365	$504 \pm 2$	38.0	9
FRB 191001	0.234	$506.92 \pm 0.04$	44.7	9
FRB 191228	0.2432	$297.5 \pm 0.05$	33.0	2
FRB 200430	0.16	$380.1 \pm 0.4$	27.0	9
FRB 200906	0.3688	$577.8 \pm 0.02$	36.0	2
FRB 201124	0.098	$413.52 \pm 0.05$	123.2	11

NOTE—References: (1) Chatterjee et al. (2017); (2) Bhandari et al. (2022); (3) Marcote et al. (2020); (4) Bannister et al. (2019); (5) Prochaska et al. (2019); (6) Bhandari et al. (2020); (7) Ravi et al. (2019); (8) Chittidi et al. (2021); (9) Heintz et al. (2020); (10) Law et al. (2020); (11) Ravi et al. (2022).

To construct a likelihood function  $\mathcal{L}$  from FRB measurements, we build a model for  $\text{DM}_{\text{IGM}}$ . The model probability distribution for  $\text{DM}_{\text{IGM}}$  has been derived from the theoretical treatments of the IGM and galaxy halos with a standard deviation  $\sigma_{\text{DM}}$  dominated by the variance in  $\text{DM}_{\text{IGM}}$ . The  $\text{DM}_{\text{IGM}}$  distributions derived in both semi-analytic models and cosmological simulations can be well fitted by a quasi-Gaussian function with a long tail (McQuinn 2014; Prochaska & Zheng 2019; Macquart et al. 2020)

$$P_{\text{IGM}}(\Delta) = A\Delta^{-\beta} \exp\left[-\frac{(\Delta^{-\epsilon} - C_0)^2}{2\epsilon^2\sigma_{\text{DM}}^2}\right], \quad \Delta > 0, \quad (5)$$

where  $\Delta \equiv \text{DM}_{\text{IGM}} / \langle \text{DM}_{\text{IGM}} \rangle$ ,  $A$  is a normalization coefficient, and the indices  $\epsilon$  and  $\beta$  are related to the inner density profile of gas in halos. Here we take  $\epsilon = 3$  and  $\beta = 3$ , as Macquart et al. (2020) did in their treatment.  $C_0$  is a free parameter, which can be fitted when the mean  $\langle \Delta \rangle = 1$ . The motivation for this analytic form (Equation (5)) is that in the limit of small  $\sigma_{\text{DM}}$ , the  $\text{DM}_{\text{IGM}}$  distribution should approach a Gaussian owing to the more diffuse halo gas and the Gaussianity of structure on large scales. Conversely, when the variance is large, this probability distribution captures the large skew that due to a few large structures that contribute to the DM of many sightlines. Recently, Zhang et al. (2021) used the IllustrisTNG simulation to estimate the probability distributions of  $\text{DM}_{\text{IGM}}$  at different redshifts realistically. Following Wu et al. (2022), the best-fit parameters ( $A$ ,  $C_0$ , and  $\sigma_{\text{DM}}$ ) of the  $\text{DM}_{\text{IGM}}$  distributions at the different redshifts that presented by Zhang et al. (2021) are used for our purpose. The uncertainties of these best-fit parameters may impact our final  $f_{\text{IGM}}$  constraint. To investigate whether the uncertainties of these parameters affect the  $\Omega_b$  constraint (similar to our  $f_{\text{IGM}}$  constraint), Yang et al. (2022) derived  $\Omega_b$  using the best-fit values of these parameters plus or minus the uncertainties. They found that these uncertainties have almost no effect on the final  $\Omega_b$  constraint. Given the fact that our  $f_{\text{IGM}}$  constraint is almost the same as that of Yang et al. (2022), we can come to the same conclusion. Note that since the  $\text{DM}_{\text{IGM}}$  distributions are given in discrete redshifts (Zhang et al. 2021), we extrapolate them to the redshifts of the localized FRBs through cubic spline interpolation.

Given the model for  $\text{DM}_{\text{IGM}}$ , we estimate the likelihood function by computing the joint likelihoods of 17 FRBs (Macquart et al. 2020):

$$\mathcal{L}_{\text{FRB}} = \prod_{i=1}^{N_{\text{FRB}}} P_i(\text{DM}_{\text{E},i}), \quad (6)$$

where  $P_i(\text{DM}_{\text{E},i})$  is the probability of the total observed  $\text{DM}_{\text{obs}}$  corrected for our galaxy, i.e.,  $\text{DM}_{\text{E}} \equiv \text{DM}_{\text{obs}} - \text{DM}_{\text{ISM}}^{\text{MW}} - \text{DM}_{\text{halo}}^{\text{MW}} = \text{DM}_{\text{IGM}} + \text{DM}_{\text{host}}/(1+z)$ . For a burst at

redshift  $z_i$ , we have

$$P_i(\text{DM}_{\text{E},i}) = \int_0^{\text{DM}_{\text{E},i}} P_{\text{host}}(\text{DM}_{\text{host}}) \times P_{\text{IGM}}(\text{DM}_{\text{E},i} - \text{DM}_{\text{host},z_i}) d\text{DM}_{\text{host}}, \quad (7)$$

where the probability density functions for  $P_{\text{host}}(\text{DM}_{\text{host}})$  and  $P_{\text{IGM}}(\text{DM}_{\text{IGM}})$  are obtained from Equations (4) and (5), respectively. Note that the Milky Way halo DM distribution ( $\text{DM}_{\text{halo}}^{\text{MW}}$ ) will be considered as a free parameter in our analysis. We will marginalize  $\text{DM}_{\text{halo}}^{\text{MW}}$  using a Gaussian prior of  $\text{DM}_{\text{halo}}^{\text{MW}} = 65 \pm 15 \text{ pc cm}^{-3}$  over the range of  $[\mu_{\text{halo}} - 3\sigma_{\text{halo}}, \mu_{\text{halo}} + 3\sigma_{\text{halo}}]$ , where  $\mu_{\text{halo}} = 65 \text{ pc cm}^{-3}$  and  $\sigma_{\text{halo}} = 15 \text{ pc cm}^{-3}$  (see Equation (3)).

### 3. OTHER COSMOLOGICAL PROBES

As we discussed in Section 1, in order to break the degeneracy between the IGM baryon fraction  $f_{\text{IGM}}$  and other cosmological parameters ( $\Omega_m$ ,  $\Omega_b$ , and  $H_0$ ; see Equation (2)), we use up-to-date cosmological data compilations, including SNe Ia, BAO, and CMB data. The exact compilations and the details for the likelihoods are described separately in what follows.

#### 3.1. Type Ia Supernovae

The SNe Ia dataset that we use in this work is the Pantheon sample, which consists of 1048 SNe Ia in the redshift range  $0.01 < z < 2.3$  (Scolnic et al. 2018). The observed distance modulus of each SN is given as

$$\mu_{\text{SN}} = m_{\text{corr}} - M_B, \quad (8)$$

where  $m_{\text{corr}}$  is the corrected apparent magnitude and  $M_B$  is the absolute magnitude.

The theoretical distance modulus  $\mu_{\text{th}}(z)$  is defined as

$$\mu_{\text{th}} = 5 \log_{10} \left[ \frac{d_L(z)}{\text{Mpc}} \right] + 25, \quad (9)$$

where  $d_L(z) = (1+z) \frac{c}{H_0} \int_0^z \frac{dz'}{\sqrt{\Omega_m(1+z')^3 + 1 - \Omega_m}}$  is the luminosity distance in the flat  $\Lambda$ CDM model. Thus, the  $\chi_{\text{SN}}^2$  function for the Pantheon data is

$$\chi_{\text{SN}}^2 = \Delta \hat{\mu}^T \cdot \mathbf{C}_{\text{SN}}^{-1} \cdot \Delta \hat{\mu}, \quad (10)$$

where  $\Delta \hat{\mu} = \hat{\mu}_{\text{SN}} - \hat{\mu}_{\text{th}}$  is the data vector, defined by the difference between the SN distance modulus  $\mu_{\text{SN}}$  and the theoretical distance modulus  $\mu_{\text{th}}$ , and  $\mathbf{C}_{\text{SN}}$  is the covariance matrix that contains both statistical and systematic uncertainties of SNe.

#### 3.2. Baryon Acoustic Oscillations

Primordial perturbations in the early universe excite acoustic waves in the plasma, known as BAO. After the recombination period, the propagation of acoustic waves was frozen.



Thus, there is a characteristic scale called the comoving sound horizon  $r_s$ , which can be approximated as (Aubourg et al. 2015)

$$r_s(z^*) = \int_{z^*}^{\infty} \frac{c_s(z)}{H(z)} dz \approx \frac{55.154 \exp[-72.3 (\Omega_b h^2 + 0.0006)^2]}{(\Omega_b h^2)^{0.12807} (\Omega_m h^2)^{0.25351}} \text{ Mpc}, \quad (11)$$

where  $c_s(z)$  is the sound speed of the photon-baryon fluid,  $z$  is the redshift at the drag epoch,  $\Omega_b$  is the present-day neutrino density, and  $h \equiv H_0/(100 \text{ km s}^{-1} \text{ Mpc}^{-1})$  is the reduced Hubble constant. Here we use a combination of 11 BAO measurements from Ryan et al. (2019). Six of these BAO measurements are correlated, in which case  $\chi^2$  is given by

$$\chi_{\text{BAO1}}^2 = (\mathbf{A}_{\text{obs}} - \mathbf{A}_{\text{th}})^T \cdot \mathbf{C}_{\text{BAO}}^{-1} \cdot (\mathbf{A}_{\text{obs}} - \mathbf{A}_{\text{th}}), \quad (12)$$

where  $\mathbf{A}_{\text{obs}}$  ( $\mathbf{A}_{\text{th}}$ ) is the vector that contains all of the six measured (theoretical) values and  $\mathbf{C}_{\text{BAO}}$  is the covariance matrix for the BAO data sets. The other five BAO measurements are uncorrelated, so

$$\chi_{\text{BAO2}}^2 = \sum_{i=1}^5 \frac{[A_{\text{th}}(z_i) - A_{\text{obs}}(z_i)]^2}{\sigma_i^2}, \quad (13)$$

where  $\sigma_i$  is the standard deviation of the  $i$ -th BAO measurement  $A_{\text{obs}}(z_i)$ . The data are combined into a  $\chi^2$ -statistic  $\chi_{\text{BAO}}^2 = \chi_{\text{BAO1}}^2 + \chi_{\text{BAO2}}^2$ .

### 3.3. Cosmic Microwave Background

For the CMB measurements, we use the derived parameters, including the acoustic scale  $l_A$ , the shift parameter  $R$ , and  $\Omega_b h^2$  from the Planck analysis of the CMB (TT, TE, EE + lowE) (Chen et al. 2019; Planck Collaboration et al. 2020). The acoustic scale is

$$l_A(z^*) = (1+z^*) \frac{\pi d_A(z^*)}{r_s(z^*)}, \quad (14)$$

where  $r_s$  is the comoving sound horizon at the recombination and  $d_A = d_L(1+z)^{-2}$  is the angular diameter distance. The shift parameter is

$$R(z^*) = (1+z^*) \frac{d_A(z^*) \sqrt{\Omega_m H_0}}{c}. \quad (15)$$

The redshift at decoupling  $z^*$  is given by

$$z^* = 1048 \left[ 1 + 0.00124 (\Omega_b h^2)^{-0.738} \right] \left[ 1 + g_1 (\Omega_m h^2)^{g_2} \right], \quad (16)$$

$$g_1 = \frac{0.0738 (\Omega_b h^2)^{-0.238}}{1 + 39.5 (\Omega_b h^2)^{0.763}}, \quad (17)$$

$$g_2 = \frac{0.560}{1 + 21.1 (\Omega_b h^2)^{1.81}}. \quad (18)$$

By setting  $x = (R, l_A, \Omega_b h^2)$ , the  $\chi_{\text{CMB}}^2$  value for the CMB data is then

$$\chi_{\text{CMB}}^2 = (x_{\text{obs}} - x_{\text{th}})^T \cdot \mathbf{C}_{\text{CMB}}^{-1} \cdot (x_{\text{obs}} - x_{\text{th}}), \quad (19)$$

where  $x_{\text{obs}} = (1.7502, 301.471, 0.02236)$  and  $x_{\text{th}}$  contain the observed and theoretical values of the derived parameters, respectively, and  $\mathbf{C}_{\text{CMB}}$  is the covariance matrix for the CMB data. Note that the distance priors derived from the CMB data are dependent on the specific cosmological model. Here we adopt the values of  $x_{\text{obs}}$  and  $\mathbf{C}_{\text{CMB}}$  that inferred from the flat  $\Lambda$ CDM model.

## 4. PARAMETER ESTIMATE AND RESULTS

To assess how well localized FRBs may help to constrain the evolution of the IGM baryon fraction  $f_{\text{IGM}}(z)$ , we consider two different parametric models. First, a simple constant model,

$$f_{\text{IGM}} = f_{\text{IGM},0}. \quad (20)$$

And second, a time-dependent model given by

$$f_{\text{IGM}}(z) = f_{\text{IGM},0} \left( 1 + \alpha \frac{z}{1+z} \right), \quad (21)$$

where  $f_{\text{IGM},0}$  is the present value of  $f_{\text{IGM}}$  and  $\alpha$  quantifies any possible evolution of  $f_{\text{IGM}}$ . As massive halos are more abundant in the late universe,  $f_{\text{IGM}}$  is believed to grow with redshift (McQuinn 2014; Prochaska & Zheng 2019). Therefore, here we require  $\alpha \geq 0$ .

The quantities  $f_{\text{IGM}}(z)$ ,  $\Omega_m$ ,  $\Omega_b h^2$ ,  $H_0$ ,  $M_B$ , and  $\text{DM}_{\text{halo}}^{\text{MW}}$  are fitted to the FRB, SN Ia, BAO, and CMB data simultaneously using the Python MCMC module *emcee* (Foreman-Mackey et al. 2013). Given the relation  $\mathcal{L} \propto \exp[-\chi^2/2]$ , the final log-likelihood sampled by *emcee* is a sum of the separated likelihoods of FRBs, SNe Ia, BAO, and CMB:

$$\ln \mathcal{L}_{\text{tot}} = \ln \mathcal{L}_{\text{FRB}} - \chi_{\text{SN}}^2/2 - \chi_{\text{BAO}}^2/2 - \chi_{\text{CMB}}^2/2. \quad (22)$$

In our baseline analysis, we set flat priors on  $f_{\text{IGM},0} \in [0, 1]$  and  $\alpha \in [0, 2]$ , and a Gaussian prior on  $\text{DM}_{\text{halo}}^{\text{MW}} = 65 \pm 15 \text{ pc cm}^{-3}$  over the  $3\sigma$  range of  $[20, 110] \text{ pc cm}^{-3}$ .

For the constant case, there are six free parameters, including the IGM baryon fraction  $f_{\text{IGM},0}$ , the cosmological parameters ( $\Omega_m$ ,  $\Omega_b h^2$ , and  $H_0$ ), the SN absolute magnitude  $M_B$ , and the Milky Way halo DM contribution  $\text{DM}_{\text{halo}}^{\text{MW}}$ . The 1D marginalized posterior distributions and 2D plots of the  $1-2\sigma$  confidence regions for these six parameters are displayed in Figure 2. These contours show that, at the  $1\sigma$  confidence level, the inferred parameter values are  $f_{\text{IGM},0} = 0.927 \pm$

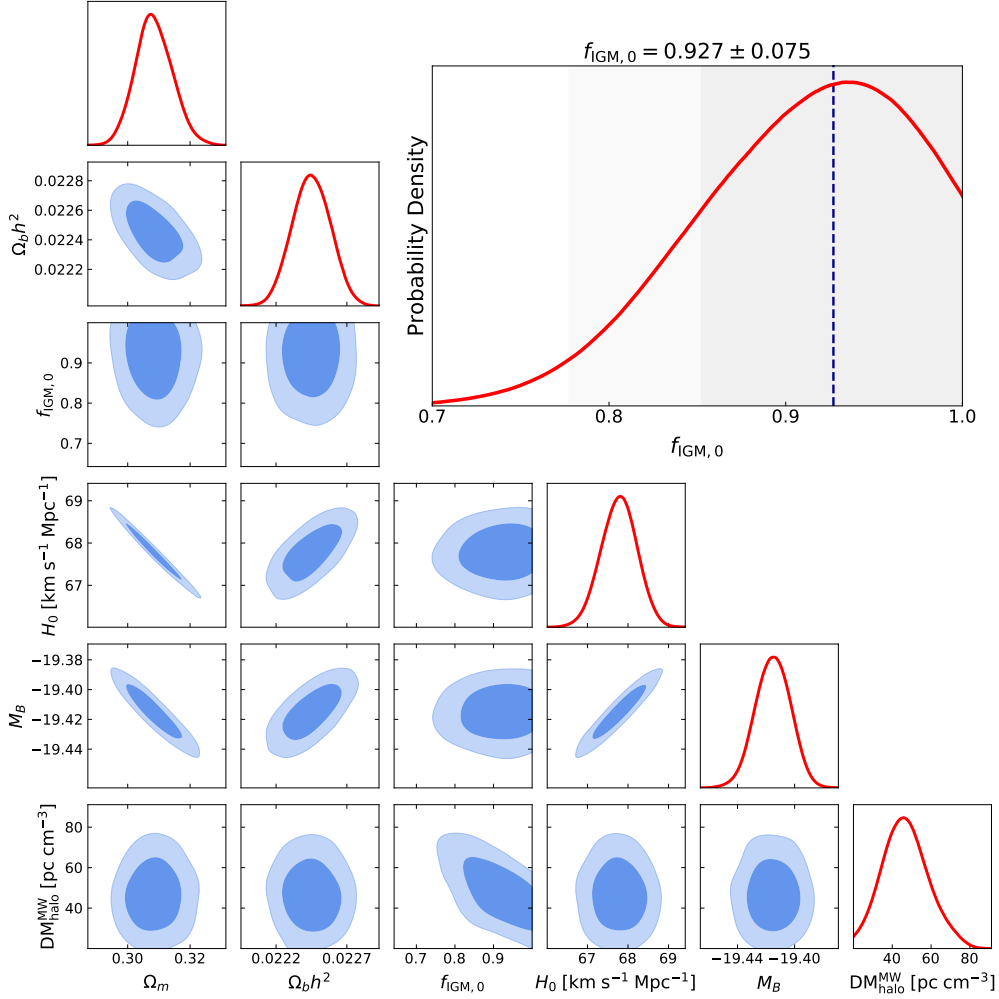


**Figure 2.** 1D and 2D marginalized posterior distributions with the  $1-2\sigma$  contours for the parameters  $f_{\text{IGM},0}$ ,  $\Omega_m$ ,  $\Omega_b h^2$ ,  $H_0$ ,  $M_B$ , and  $\text{DM}_{\text{halo}}^{\text{MW}}$  in the constant case of  $f_{\text{IGM}} = f_{\text{IGM},0}$ , constrained by the FRB, SN Ia, BAO, and CMB data. The 1D marginalized posterior distribution of  $f_{\text{IGM},0}$  is magnified on the top-right panel. The vertical dashed line represents the best fit, whereas the shaded areas correspond to the 68% and 95% confidence regions.

**Table 2.** Constraints on all parameters for two different parametric models of  $f_{\text{IGM}}$ .

Model	Constant	Time-dependent
Parameter	Estimation with 68% limits	
$f_{\text{IGM},0}$	$0.927 \pm 0.075$	$0.837 \pm 0.089$
$\alpha$	–	$< 0.882$
$\Omega_m$	$0.309 \pm 0.006$	$0.309 \pm 0.006$
$\Omega_b h^2$	$0.02245 \pm 0.00013$	$0.02245 \pm 0.00013$
$H_0 / [\text{km s}^{-1} \text{Mpc}^{-1}]$	$67.78 \pm 0.44$	$67.71 \pm 0.42$
$M_B$	$-19.415 \pm 0.012$	$-19.417 \pm 0.012$
$\text{DM}_{\text{halo}}^{\text{MW}} / [\text{pc cm}^{-3}]$	$47 \pm 10$	$49 \pm 10$
$-2 \ln \mathcal{L}_{\text{max}}$	1262.855	1263.099
$\Delta \text{AIC}$	–	2.244

$0.075$ ,  $\Omega_m = 0.309 \pm 0.006$ ,  $\Omega_b h^2 = 0.02245 \pm 0.00013$ ,  $H_0 = 67.78 \pm 0.44 \text{ km s}^{-1} \text{Mpc}^{-1}$ , and  $\text{DM}_{\text{halo}}^{\text{MW}} = 47 \pm 10 \text{ pc cm}^{-3}$ . The corresponding results are summarized in Table 2. Figure 1 also shows the theoretical curve for  $\langle \text{DM}_{\text{IGM}} \rangle$  versus  $z$  for the constant case and a model estimate of the scatter (95% interval) due to the uncertainties of the inferred parameters. The theoretical curve reflects the trend of the data well. Moreover, the inferred value of the IGM baryon fraction is compatible with previous results obtained from observations (e.g., Fukugita et al. 1998; Fukugita & Peebles 2004; Shull et al. 2012; Hill et al. 2016; Muñoz & Loeb 2018) and simulations (e.g., Cen & Ostriker 1999, 2006). The constraint accuracy of  $f_{\text{IGM},0}$  is about 8.0%.

For the time-dependent case, the free parameters are  $\{f_{\text{IGM},0}, \alpha, \Omega_m, \Omega_b h^2, H_0, M_B, \text{DM}_{\text{halo}}^{\text{MW}}\}$ . These seven parameters are constrained to be  $f_{\text{IGM},0} = 0.837 \pm 0.089$ ,  $\alpha < 0.882$ ,  $\Omega_m = 0.309 \pm 0.006$ ,  $\Omega_b h^2 = 0.02245 \pm 0.00013$ ,  $H_0 =$

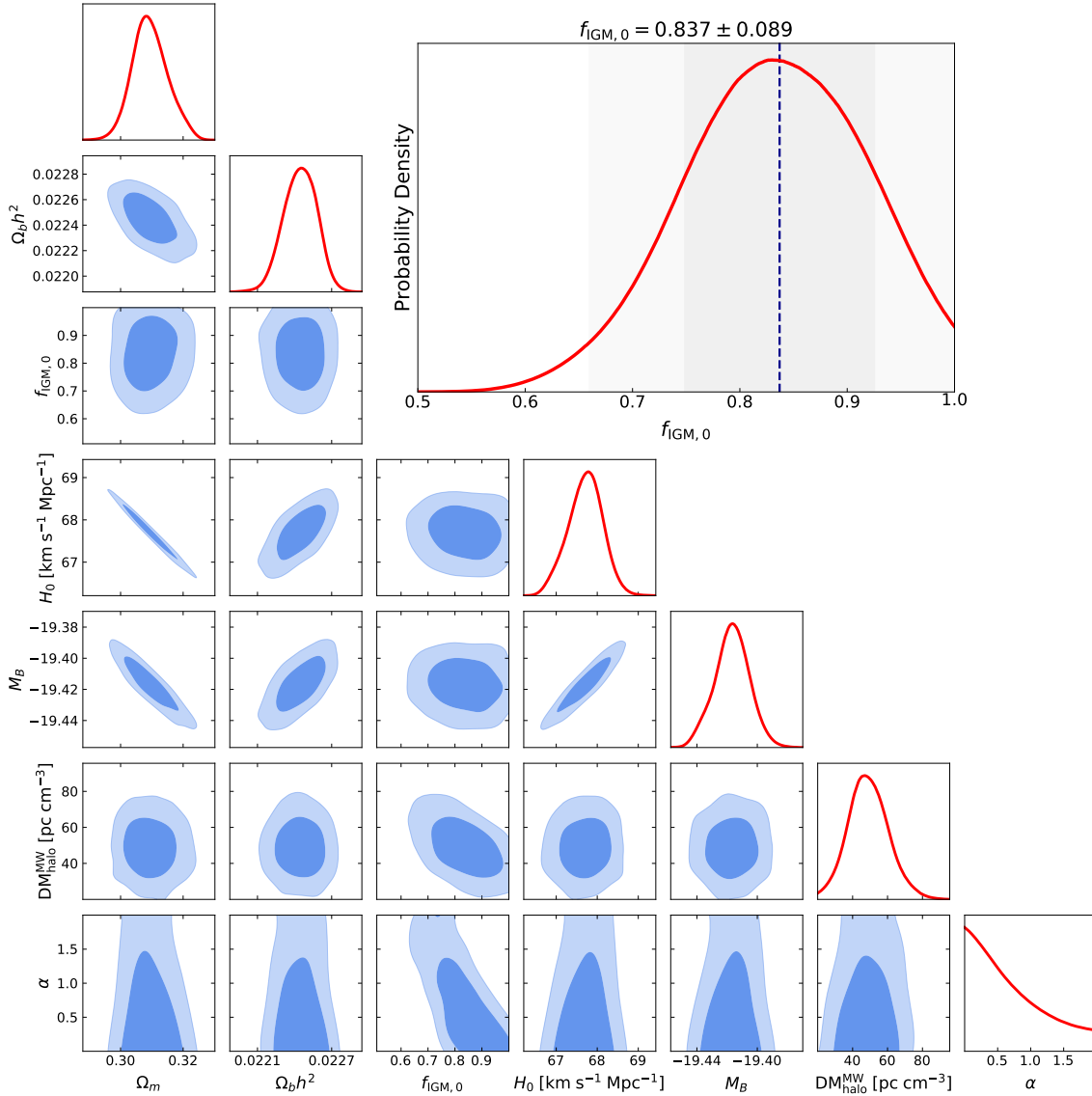


**Figure 3.** Same as Figure 2, but now for the time-dependent case of  $f_{\text{IGM}}(z) = f_{\text{IGM},0}(1 + \alpha \frac{z}{1+z})$ .

$67.71 \pm 0.42 \text{ km s}^{-1} \text{ Mpc}^{-1}$ , and  $\text{DM}_{\text{halo}}^{\text{MW}} = 49 \pm 10 \text{ pc cm}^{-3}$ , which are displayed in Figure 3 and summarized in Table 2. Note that with the requirement that  $f_{\text{IGM}}$  grows with redshift ( $\alpha \geq 0$ ), only an upper limit on  $\alpha$  can be estimated, which implies that there is no strong evidence for the redshift dependence of  $f_{\text{IGM}}$ . This is consistent with the cosmology-insensitive result obtained from five localized FRBs (Li et al. 2020). The comparison between columns 2 and 3 of Table 2 suggests that the nuisance parameters ( $\Omega_m$ ,  $\Omega_b h^2$ ,  $H_0$ ,  $M_B$ , and  $\text{DM}_{\text{halo}}^{\text{MW}}$ ) are almost identical and have little effect on the adopted parametric model of  $f_{\text{IGM}}$ .

Because the constant model and the time-dependent model do not have the same number of free parameters, a comparison of the likelihoods for either being closer to the correct model must be based on model selection criteria. We use the

Akaike Information Criterion (AIC; Akaike 1974, 1981) to test the statistical performance of the models,  $\text{AIC} = -2 \ln \mathcal{L} + 2p$ , where  $p$  is the number of free parameters. With  $\text{AIC}_1$  and  $\text{AIC}_2$  characterizing models  $\mathcal{M}_1$  (the constant model) and  $\mathcal{M}_2$  (the time-dependent model), respectively, the difference  $\Delta \text{AIC} \equiv \text{AIC}_2 - \text{AIC}_1$  determines the extent to which  $\mathcal{M}_1$  is favoured over  $\mathcal{M}_2$ . The evidence of  $\mathcal{M}_1$  being correct is judged ‘weak’ when the outcome  $\Delta \equiv \text{AIC}_2 - \text{AIC}_1$  is in the range  $0 < \Delta < 2$ , ‘positive’ when  $2 < \Delta < 6$ , and ‘strong’ when  $\Delta > 6$ . Therefore, the outcome  $\Delta \text{AIC} = 2.244$  shows a positive evidence in favor of the constant model ( $\mathcal{M}_1$ ) with respect to the time-dependent model ( $\mathcal{M}_2$ ). Nevertheless, we hold the opinion that this positive evidence may be due to the relatively low redshifts in the FRB data. To distinguish between the constant and time-dependent models bet-

ter, a larger number of FRBs localized at higher redshifts is required in the future.

In our analysis, the  $DM_{ISM}^{MW}$  values are estimated from the Galactic electron density model of NE2001 (Cordes & Lazio 2002). We also perform a parallel comparative analysis of the FRB data using the YMW16 model (Yao et al. 2017). The resulting constraints now turn to be  $f_{IGM,0} = 0.901 \pm 0.081$  ( $f_{IGM,0} = 0.788^{+0.082}_{-0.100}$ ) for the constant (time-dependent) case. Comparing these inferred  $f_{IGM,0}$  with those obtained using the NE2001 model, we see that the adoption of a different electron distribution model has a minimal influence on the results. Due to the larger  $DM_{ISM}^{MW}$  contribution at low Galactic latitudes in the YMW16 Model, the derived  $f_{IGM,0}$  values are slightly smaller than those in the NE2001 model.

To make a direct comparison with previous works, in Figure 4 we plot some typical  $f_{IGM,0}$  constraints from different FRB samples, as well as our constraints from both the NE2001 and YMW16 models. One can see from Figure 4 that our  $f_{IGM,0}$  constraints are well consistent with previous results at the  $1\sigma$  confidence level.

## 5. CONCLUSIONS

The  $DM_{IGM}-z$  relation of FRBs has been used for probing the baryon fraction in the IGM,  $f_{IGM}$ . However, such studies have been restricted by the strong degeneracy between cosmological parameters and  $f_{IGM}$ . Moreover, the DM contribution from the IGM ( $DM_{IGM}$ ) cannot be effectively distinguished from other DMs contributed by the Milky Way or host galaxy. In this work, we investigate precise constraints on  $f_{IGM}$  from the DM measurements of seventeen localized FRBs. In order to break the parameter degeneracy, we combine FRB data with three other cosmological probes (including SNe Ia, BAO, and CMB) to infer cosmological parameters and  $f_{IGM}$  simultaneously. To avoid uncontrollable systematic errors induced by the  $DM_{IGM}$  deduction, we handle the DM contributions of the host galaxies and IGM as the probability distributions derived from the the IllustrisTNG simulation.

Following the analysis method described in Section 2, we explore the possible redshift dependence of  $f_{IGM}(z)$  considering two different parametric models, which are expressed as the constant and time-dependent parameterizations given by Equations (20) and (21). The MCMC analysis is used to constrain  $f_{IGM}(z)$  and other cosmological parameters. For the constant model, we infer that  $f_{IGM,0} = 0.927 \pm 0.075$ , repre-

senting a precision of 8.0%. This constraint from FRB observations is roughly consistent with those obtained from other probes (Fukugita et al. 1998; Fukugita & Peebles 2004; Shull et al. 2012; Hill et al. 2016). For the time-dependent model, whereas only an upper limit on the evolution index  $\alpha$  can be set ( $\alpha < 0.882$ ), we can obtain a good limit on the local  $f_{IGM,0} = 0.837 \pm 0.089$ , which is slightly looser but still consistent with previous results derived from different methods. According to the AIC model selection criteria, there is a mild evidence suggesting that the constant model is preferred over the time-dependent model. However, due to the fact that the number of current localized FRBs is small and their redshift measurements are relatively low, we cannot safely exclude the possibility of an evolving  $f_{IGM}(z)$ .

Redshift measurements of a larger sample of FRBs are essential for using this method presented here to constrain  $f_{IGM}$  and its possible redshift evolution. Forthcoming radio telescopes such as the Deep Synoptic Array 2000-dish prototype (Hallinan et al. 2019) and the Square Kilometre Array (Dewdney et al. 2009), with improved detection sensitivity and localization capability, will be able to increase the current localized FRB sample size by orders of magnitude. With the rapid progress in localizing FRBs, the constraints on  $f_{IGM}$  will be significantly improved, and the baryon distribution of the universe will be better understood.

1 We are grateful to the anonymous referee for their help-  
 2 ful comments. This work is partially supported by the Na-  
 3 tional Key Research and Development Program of China  
 4 (2022SKA0130100), the National Natural Science Foun-  
 5 dation of China (grant Nos. 11725314 and 12041306),  
 6 the Key Research Program of Frontier Sciences (grant No.  
 7 ZDBS-LY-7014) of Chinese Academy of Sciences, Inter-  
 8 national Partnership Program of Chinese Academy of Sci-  
 9 ences for Grand Challenges (114332KYSB20210018), the  
 10 CAS Project for Young Scientists in Basic Research (grant  
 11 No. YSBR-063), the CAS Organizational Scientific Re-  
 12 search Platform for National Major Scientific and Techno-  
 13 logical Infrastructure: Cosmic Transients with FAST, the  
 14 Natural Science Foundation of Jiangsu Province (grant No.  
 15 BK20221562), and the Young Elite Scientists Sponsorship  
 16 Program of Jiangsu Association for Science and Technol-  
 17 ogy.

## REFERENCES

- Akaike, H. 1974, IEEE transactions on automatic control, 19, 716  
 —. 1981, Journal of econometrics, 16, 3  
 Aubourg, É., Bailey, S., Bautista, J. E., et al. 2015, PhRvD, 92,  
 123516, doi: [10.1103/PhysRevD.92.123516](https://doi.org/10.1103/PhysRevD.92.123516)  
 Bannister, K. W., Deller, A. T., Phillips, C., et al. 2019, Science,  
 365, 565, doi: [10.1126/science.aaw5903](https://doi.org/10.1126/science.aaw5903)



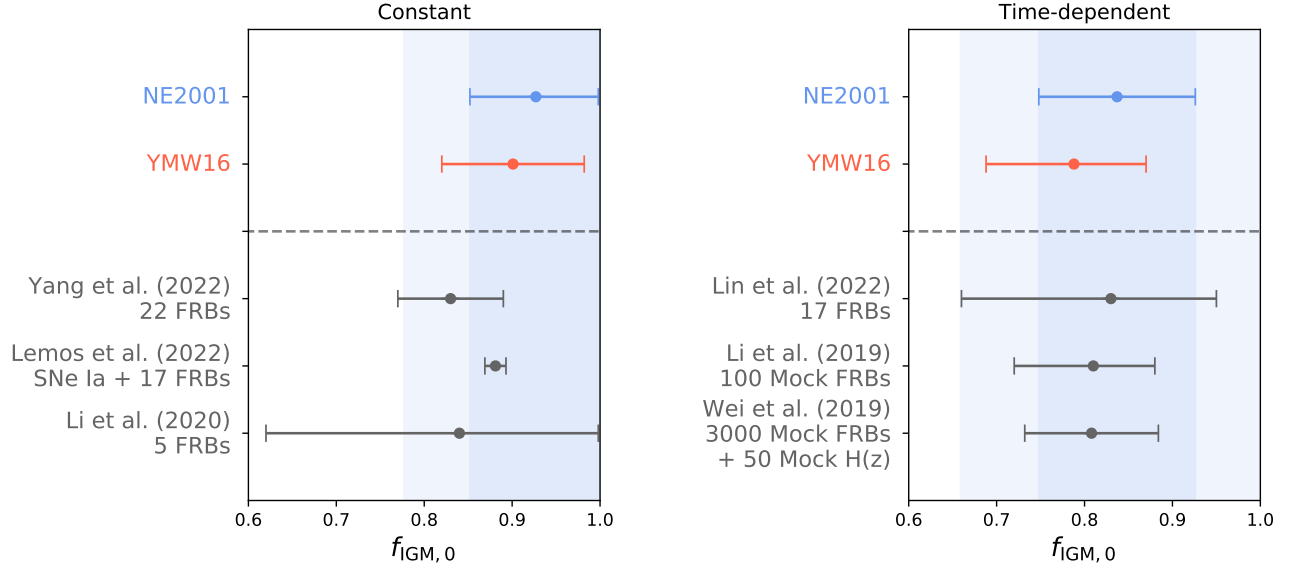


**Figure 4.** Comparison of  $f_{\text{IGM},0}$  constraints with previous results in the constant (left panel) and time-dependent (right panel) cases. The shaded areas in both panels represent the  $1\sigma$  and  $2\sigma$  confidence regions of the corresponding  $f_{\text{IGM},0}$  constraints.

Becker, G. D., Bolton, J. S., Haehnelt, M. G., & Sargent, W. L. W. 2011, MNRAS, 410, 1096,

doi: [10.1111/j.1365-2966.2010.17507.x](https://doi.org/10.1111/j.1365-2966.2010.17507.x)

Bhandari, S., Sadler, E. M., Prochaska, J. X., et al. 2020, ApJL, 895, L37, doi: [10.3847/2041-8213/ab672e](https://doi.org/10.3847/2041-8213/ab672e)

Bhandari, S., Heintz, K. E., Aggarwal, K., et al. 2022, AJ, 163, 69, doi: [10.3847/1538-3881/ac3aac](https://doi.org/10.3847/1538-3881/ac3aac)

Bhardwaj, M., Kirichenko, A. Y., Michilli, D., et al. 2021a, ApJL, 919, L24, doi: [10.3847/2041-8213/ac223b](https://doi.org/10.3847/2041-8213/ac223b)

Bhardwaj, M., Gaensler, B. M., Kaspi, V. M., et al. 2021b, ApJL, 910, L18, doi: [10.3847/2041-8213/abeaa6](https://doi.org/10.3847/2041-8213/abeaa6)

Cen, R., & Ostriker, J. P. 1999, ApJ, 514, 1, doi: [10.1086/306949](https://doi.org/10.1086/306949)

—, 2006, ApJ, 650, 560, doi: [10.1086/506505](https://doi.org/10.1086/506505)

Chatterjee, S., Law, C. J., Wharton, R. S., et al. 2017, Nature, 541, 58, doi: [10.1038/nature20797](https://doi.org/10.1038/nature20797)

Chen, L., Huang, Q.-G., & Wang, K. 2019, JCAP, 2019, 028, doi: [10.1088/1475-7516/2019/02/028](https://doi.org/10.1088/1475-7516/2019/02/028)

CHIME/FRB Collaboration, Amiri, M., Andersen, B. C., et al. 2021, ApJS, 257, 59, doi: [10.3847/1538-4365/ac33ab](https://doi.org/10.3847/1538-4365/ac33ab)

Chittidi, J. S., Simha, S., Mannings, A., et al. 2021, ApJ, 922, 173, doi: [10.3847/1538-4357/ac2818](https://doi.org/10.3847/1538-4357/ac2818)

Cordes, J. M., & Lazio, T. J. W. 2002, arXiv e-prints, astro, <https://arxiv.org/abs/astro-ph/0207156>

Dai, J.-P., & Xia, J.-Q. 2021, MNRAS, 503, 4576, doi: [10.1093/mnras/stab785](https://doi.org/10.1093/mnras/stab785)

Deng, W., & Zhang, B. 2014, ApJL, 783, L35, doi: [10.1088/2041-8205/783/2/L35](https://doi.org/10.1088/2041-8205/783/2/L35)

Dewdney, P. E., Hall, P. J., Schilizzi, R. T., & Lazio, T. J. L. W. 2009, IEEE Proceedings, 97, 1482, doi: [10.1109/JPROC.2009.2021005](https://doi.org/10.1109/JPROC.2009.2021005)

Foreman-Mackey, D., Hogg, D. W., Lang, D., & Goodman, J. 2013, PASP, 125, 306, doi: [10.1086/670067](https://doi.org/10.1086/670067)

Fukugita, M., Hogan, C. J., & Peebles, P. J. E. 1998, ApJ, 503, 518, doi: [10.1086/306025](https://doi.org/10.1086/306025)

Fukugita, M., & Peebles, P. J. E. 2004, ApJ, 616, 643, doi: [10.1086/425155](https://doi.org/10.1086/425155)

Gao, H., Li, Z., & Zhang, B. 2014, ApJ, 788, 189, doi: [10.1088/0004-637X/788/2/189](https://doi.org/10.1088/0004-637X/788/2/189)

Hagstotz, S., Reischke, R., & Lilow, R. 2022, MNRAS, 511, 662, doi: [10.1093/mnras/stac077](https://doi.org/10.1093/mnras/stac077)

Hallinan, G., Ravi, V., Weinreb, S., et al. 2019, in Bulletin of the American Astronomical Society, Vol. 51, 255.

<https://arxiv.org/abs/1907.07648>

Hashimoto, T., Goto, T., Lu, T.-Y., et al. 2021, MNRAS, 502, 2346, doi: [10.1093/mnras/stab186](https://doi.org/10.1093/mnras/stab186)

Heintz, K. E., Prochaska, J. X., Simha, S., et al. 2020, ApJ, 903, 152, doi: [10.3847/1538-4357/abb6fb](https://doi.org/10.3847/1538-4357/abb6fb)

Hill, J. C., Ferraro, S., Battaglia, N., Liu, J., & Spergel, D. N. 2016, PhRvL, 117, 051301, doi: [10.1103/PhysRevLett.117.051301](https://doi.org/10.1103/PhysRevLett.117.051301)

Jaroszynski, M. 2019, MNRAS, 484, 1637, doi: [10.1093/mnras/sty3529](https://doi.org/10.1093/mnras/sty3529)

Kirsten, F., Marcote, B., Nimmo, K., et al. 2022, Nature, 602, 585, doi: [10.1038/s41586-021-04354-w](https://doi.org/10.1038/s41586-021-04354-w)

Kumar, P., & Linder, E. V. 2019, PhRvD, 100, 083533, doi: [10.1103/PhysRevD.100.083533](https://doi.org/10.1103/PhysRevD.100.083533)

Law, C. J., Butler, B. J., Prochaska, J. X., et al. 2020, ApJ, 899, 161, doi: [10.3847/1538-4357/aba4ac](https://doi.org/10.3847/1538-4357/aba4ac)

Lemos, T., Gonçalves, R. S., Carvalho, J. C., & Alcaniz, J. S. 2022, arXiv e-prints, arXiv:2205.07926.

<https://arxiv.org/abs/2205.07926>

- Li, Z., Gao, H., Wei, J.-J., et al. 2019, *ApJ*, 876, 146, doi: [10.3847/1538-4357/ab18fe](https://doi.org/10.3847/1538-4357/ab18fe)
- Li, Z., Gao, H., Wei, J. J., et al. 2020, *MNRAS*, 496, L28, doi: [10.1093/mnras/slao070](https://doi.org/10.1093/mnras/slao070)
- Li, Z.-X., Gao, H., Ding, X.-H., Wang, G.-J., & Zhang, B. 2018, *Nature Communications*, 9, 3833, doi: [10.1038/s41467-018-06303-0](https://doi.org/10.1038/s41467-018-06303-0)
- Lin, H.-N., Li, X., & Tang, L. 2022, *Chinese Physics C*, 46, 075102, doi: [10.1088/1674-1137/ac5e92](https://doi.org/10.1088/1674-1137/ac5e92)
- Lorimer, D. R., Bailes, M., McLaughlin, M. A., Narkevic, D. J., & Crawford, F. 2007, *Science*, 318, 777, doi: [10.1126/science.1147532](https://doi.org/10.1126/science.1147532)
- Macquart, J. P., Prochaska, J. X., McQuinn, M., et al. 2020, *Nature*, 581, 391, doi: [10.1038/s41586-020-2300-2](https://doi.org/10.1038/s41586-020-2300-2)
- Marcote, B., Nimmo, K., Hessels, J. W. T., et al. 2020, *Nature*, 577, 190, doi: [10.1038/s41586-019-1866-z](https://doi.org/10.1038/s41586-019-1866-z)
- McQuinn, M. 2014, *ApJL*, 780, L33, doi: [10.1088/2041-8205/780/2/L33](https://doi.org/10.1088/2041-8205/780/2/L33)
- Meiksin, A. A. 2009, *Reviews of Modern Physics*, 81, 1405, doi: [10.1103/RevModPhys.81.1405](https://doi.org/10.1103/RevModPhys.81.1405)
- Muñoz, J. B., Kovetz, E. D., Dai, L., & Kamionkowski, M. 2016, *PhRvL*, 117, 091301, doi: [10.1103/PhysRevLett.117.091301](https://doi.org/10.1103/PhysRevLett.117.091301)
- Muñoz, J. B., & Loeb, A. 2018, *PhRvD*, 98, 103518, doi: [10.1103/PhysRevD.98.103518](https://doi.org/10.1103/PhysRevD.98.103518)
- Niu, C. H., Aggarwal, K., Li, D., et al. 2022, *Nature*, 606, 873, doi: [10.1038/s41586-022-04755-5](https://doi.org/10.1038/s41586-022-04755-5)
- Petroff, E., Barr, E. D., Jameson, A., et al. 2016, *PASA*, 33, e045, doi: [10.1017/pasa.2016.35](https://doi.org/10.1017/pasa.2016.35)
- Planck Collaboration, Aghanim, N., Akrami, Y., et al. 2020, *A&A*, 641, A6, doi: [10.1051/0004-6361/201833910](https://doi.org/10.1051/0004-6361/201833910)
- Platts, E., Weltman, A., Walters, A., et al. 2019, *PhR*, 821, 1, doi: [10.1016/j.physrep.2019.06.003](https://doi.org/10.1016/j.physrep.2019.06.003)
- Prochaska, J. X., & Zheng, Y. 2019, *MNRAS*, 485, 648, doi: [10.1093/mnras/stz261](https://doi.org/10.1093/mnras/stz261)
- Prochaska, J. X., Macquart, J.-P., McQuinn, M., et al. 2019, *Science*, 366, 231, doi: [10.1126/science.aay0073](https://doi.org/10.1126/science.aay0073)
- Qiang, D.-C., & Wei, H. 2020, *JCAP*, 2020, 023, doi: [10.1088/1475-7516/2020/04/023](https://doi.org/10.1088/1475-7516/2020/04/023)
- Qiu, X.-W., Zhao, Z.-W., Wang, L.-F., Zhang, J.-F., & Zhang, X. 2022, *JCAP*, 2022, 006, doi: [10.1088/1475-7516/2022/02/006](https://doi.org/10.1088/1475-7516/2022/02/006)
- Ravi, V., Catha, M., D'Addario, L., et al. 2019, *Nature*, 572, 352, doi: [10.1038/s41586-019-1389-7](https://doi.org/10.1038/s41586-019-1389-7)
- Ravi, V., Law, C. J., Li, D., et al. 2022, *MNRAS*, 513, 982, doi: [10.1093/mnras/stac465](https://doi.org/10.1093/mnras/stac465)
- Ryan, J., Chen, Y., & Ratra, B. 2019, *MNRAS*, 488, 3844, doi: [10.1093/mnras/stz1966](https://doi.org/10.1093/mnras/stz1966)
- Ryder, S. D., Bannister, K. W., Bhandari, S., et al. 2022, arXiv e-prints, arXiv:2210.04680. <https://arxiv.org/abs/2210.04680>
- Scolnic, D. M., Jones, D. O., Rest, A., et al. 2018, *ApJ*, 859, 101, doi: [10.3847/1538-4357/aab9bb](https://doi.org/10.3847/1538-4357/aab9bb)
- Shull, J. M., Smith, B. D., & Danforth, C. W. 2012, *ApJ*, 759, 23, doi: [10.1088/0004-637X/759/1/23](https://doi.org/10.1088/0004-637X/759/1/23)
- Springel, V., Pakmor, R., Pillepich, A., et al. 2018, *MNRAS*, 475, 676, doi: [10.1093/mnras/stx3304](https://doi.org/10.1093/mnras/stx3304)
- Thornton, D., Stappers, B., Bailes, M., et al. 2013, *Science*, 341, 53, doi: [10.1126/science.1236789](https://doi.org/10.1126/science.1236789)
- Walters, A., Ma, Y.-Z., Sievers, J., & Weltman, A. 2019, *PhRvD*, 100, 103519, doi: [10.1103/PhysRevD.100.103519](https://doi.org/10.1103/PhysRevD.100.103519)
- Walters, A., Weltman, A., Gaensler, B. M., Ma, Y.-Z., & Witzemann, A. 2018, *ApJ*, 856, 65, doi: [10.3847/1538-4357/aaaf6b](https://doi.org/10.3847/1538-4357/aaaf6b)
- Wang, Y. K., & Wang, F. Y. 2018, *A&A*, 614, A50, doi: [10.1051/0004-6361/201731160](https://doi.org/10.1051/0004-6361/201731160)
- Wei, J.-J., Li, Z., Gao, H., & Wu, X.-F. 2019, *JCAP*, 2019, 039, doi: [10.1088/1475-7516/2019/09/039](https://doi.org/10.1088/1475-7516/2019/09/039)
- Wei, J.-J., Wu, X.-F., & Gao, H. 2018, *ApJL*, 860, L7, doi: [10.3847/2041-8213/aac8e2](https://doi.org/10.3847/2041-8213/aac8e2)
- Wu, Q., Zhang, G.-Q., & Wang, F.-Y. 2022, *MNRAS*, 515, L1, doi: [10.1093/mnras/slac022](https://doi.org/10.1093/mnras/slac022)
- Xiao, D., Wang, F., & Dai, Z. 2021, *Science China Physics, Mechanics, and Astronomy*, 64, 249501, doi: [10.1007/s11433-020-1661-7](https://doi.org/10.1007/s11433-020-1661-7)
- Yang, K. B., Wu, Q., & Wang, F. Y. 2022, *ApJL*, 940, L29, doi: [10.3847/2041-8213/aca145](https://doi.org/10.3847/2041-8213/aca145)
- Yao, J. M., Manchester, R. N., & Wang, N. 2017, *ApJ*, 835, 29, doi: [10.3847/1538-4357/835/1/29](https://doi.org/10.3847/1538-4357/835/1/29)
- Yu, H., & Wang, F. Y. 2017, *A&A*, 606, A3, doi: [10.1051/0004-6361/201731607](https://doi.org/10.1051/0004-6361/201731607)
- Zhang, B. 2022, arXiv e-prints, arXiv:2212.03972. <https://arxiv.org/abs/2212.03972>
- Zhang, G. Q., Yu, H., He, J. H., & Wang, F. Y. 2020, *ApJ*, 900, 170, doi: [10.3847/1538-4357/abaa4a](https://doi.org/10.3847/1538-4357/abaa4a)
- Zhang, Z. J., Yan, K., Li, C. M., Zhang, G. Q., & Wang, F. Y. 2021, *ApJ*, 906, 49, doi: [10.3847/1538-4357/abceb9](https://doi.org/10.3847/1538-4357/abceb9)
- Zhao, Z.-W., Li, Z.-X., Qi, J.-Z., et al. 2020, *ApJ*, 903, 83, doi: [10.3847/1538-4357/abb8ce](https://doi.org/10.3847/1538-4357/abb8ce)
- Zheng, Z., Ofek, E. O., Kulkarni, S. R., Neill, J. D., & Juric, M. 2014, *ApJ*, 797, 71, doi: [10.1088/0004-637X/797/1/71](https://doi.org/10.1088/0004-637X/797/1/71)
- Zhou, B., Li, X., Wang, T., Fan, Y.-Z., & Wei, D.-M. 2014, *PhRvD*, 89, 107303, doi: [10.1103/PhysRevD.89.107303](https://doi.org/10.1103/PhysRevD.89.107303)